ACS APPLIED MATERIALS & INTERFACES

Research Article

www.acsami.org

Poly(vinyl alcohol)/Cellulose Nanofibril Hybrid Aerogels with an Aligned Microtubular Porous Structure and Their Composites with Polydimethylsiloxane

Tianliang Zhai,[†,‡] Qifeng Zheng,[§,∥] Zhiyong Cai,[⊥] Lih-Sheng Turng,[∥,⊥] Hesheng Xia,*[,†] and Shaoqin Gong*[,‡,§,∥]

[†]State Key Laboratory of Polymer Materials Engineering, Polymer Research Institute, Sichuan University, Chengdu 610065, China
[‡]Department of Biomedical Engineering, [§]Material Science Program, [∥]Wisconsin Institute for Discovery, and [⊥]Department of Mechanical Engineering, University of Wisconsin−Madison, Madison, Wisconsin 53562, United States

ABSTRACT: Superhydrophobic poly(vinyl alcohol) (PVA)/cellulose nanofibril (CNF) aerogels with a unidirectionally aligned microtubular porous structure were prepared using a unidirectional freeze-drying process, followed by the thermal chemical vapor deposition of methyltrichlorosilane. The silanized aerogels were characterized using various techniques including scanning electron microscopy (SEM), Fourier transform infrared spectroscopy, and contact angle measurements. The structure of the aerogels fully filled with polydimethylsiloxane (PDMS) was confirmed by SEM and optical microscopy. The mechanical properties of the resulting PDMS/aerogel composites were examined using both compressive and tensile tests. The compressive and tensile Young's moduli of the fully filled PDMS/aerogel composites were more than 2-fold and 15-fold higher than those of pure PDMS. This study provides a novel alternative approach for preparing high performance polymer nanocomposites with a bicontinuous structure.

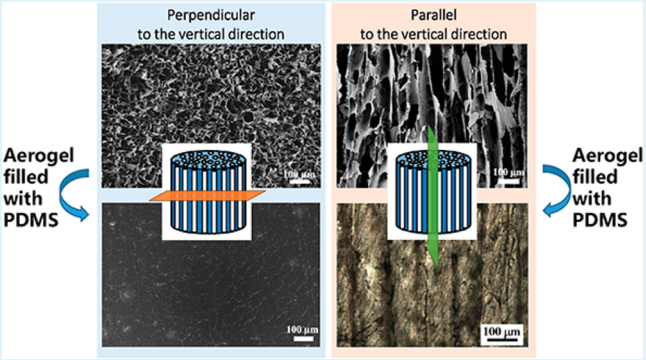

KEYWORDS: *organic aerogels, cellulose nanofibrils (CNFs), polydimethylsiloxane, unidirectional freeze-drying, mechanical properties*

INTRODUCTION

Nanoparticles often possess unique properties due to their nanoscale dimensions and high surface-to-volume ratios. Adding a small amount of nanoparticles into a polymer matrix can often significantly enhance the material properties of the polymer matrix.[1−4] As such, research on polymer nanocomposites has been very active during the last several decades. Polymer nanocomposites have shown great potential and sometimes played an irreplaceable role, in many applications such as polymer reinforcements,[1,5−7] catalytic systems,[8,9] flame retardants,[4,10,11] drug release,[12−14] energy conversion and storage,[15−17] etc.

Cellulose is considered to be the most abundant renewable natural polymer on the planet and is biodegradable and biocompatible.[18] Cellulose nanofibrils (CNFs) derived from cellulose are of particular interest due to their outstanding mechanical properties[19,20] with an elastic modulus of 140 GPa.[21] Therefore, cellulose nanofibrils can potentially be an excellent nanofiller for high-performance polymer nanocomposites, thereby presenting unprecedented opportunities to develop durable engineering materials from a renewable resource for structural, consumer, and medical applications.[6,22] There has been a long history of using plant cellulose fibers as reinforcements in polymer composite materials.[23−26] However, using nanoscale cellulose fibers to reinforce polymers has been a relatively more recent effort.[22,27−29] Despite the challenges described below, cellulose nanofibrils have been compounded with various polymer matrices, including thermoset resins,[30−32] elastomers,[33,34] polymer latexes,[35,36] water-soluble/dispersible polymers,[37−39] and biodegradable polymers.[40−43]

One major challenge with the preparation of CNF/polymer nanocomposites is that CNF is highly hydrophilic due to the nature of cellulose,[6,28] while the great majority of polymers is hydrophobic. As such, it is difficult to disperse CNFs uniformly in most of the common polymer matrices. In order to improve the compatibility between the CNFs and the hydrophobic polymer matrices, previous studies typically resorted to surface modification of CNFs utilizing physical, physico-chemical, or chemical methods.[44] Furthermore, to effectively reinforce the polymer matrix, a rigid percolating nanofiller network needs to be formed within the soft polymer matrix.[45−48] Although surface functionalization can improve the dispersion of the CNFs in the polymer matrix, uniform CNF dispersion and the formation of a rigid percolating CNF network in the polymer

Received: February 22, 2015
Accepted: March 23, 2015
Published: March 30, 2015

DOI: 10.1021/acsami.5b01679
ACS Appl. Mater. Interfaces 2015, 7, 7436−7444

matrix are still difficult to achieve during the fabrication process. Moreover, the rigid percolating filler network is highly sensitive to the type of polymer matrix and nanofiller as well as to the processing conditions.[45]

Organic aerogels possess many remarkable properties, including high porosity (typically 95% to 99%), high specific area, ultralow density, and desirable mechanical properties.[49−51] Therefore, aerogels may act as a preformed, rigid, and continuous reinforcing network for aerogel/polymer composites. Unlike the traditional polymer nanocomposites, where nanofillers are directly mixed with the molten polymer matrix, utilization of a porous aerogel scaffold allows for better control over the distribution of the reinforcing nanofiller (i.e., CNFs) and the microstructure of the resulting aerogel/polymer composites.

Here we demonstrate a polymer nanocomposite consisting of a poly(vinyl alcohol) (PVA)/CNF hybrid organic aerogel as a continuous reinforcing phase and polydimethylsiloxane (PDMS) as a polymer matrix. A unidirectional freeze-drying process, which is a promising and novel technique for creating orientational porous structures,[52−54] was used to prepare PVA/CNF aerogels with aligned microtubular porous structures. These aligned microtubular-like pores present in the PVA/CNF aerogels provide numerous microchannels for PDMS flowing into the aerogel network, thus making it possible to completely fill the porous aerogels. To facilitate the PDMS filling process, the hydrophilic surface of the PVA/CNF aerogel was rendered to be superhydrophobic via silanization using a simple thermal chemical vapor deposition process. The compressive and tensile Young's moduli of the resulting PDMS/aerogel composites were more than 2-fold and 15-fold higher than those of pure PDMS, respectively. This study provides a novel alternative approach to preparing high performance polymer nanocomposites with a bicontinuous structure.

EXPERIMENTAL SECTION

Preparation of Cellulose Nanofibrils (CNFs). TEMPO-oxidized CNFs used in this work were prepared according to the procedure reported previously.[55] The concentration of as-prepared CNFs was 0.74 wt %, and the CNF suspensions were stored at 4 °C without any treatment before future utilization.

Preparation of PVA Solution. PVA (20.0 g, MW: 95 000 g mol^{-1}, Sigma-Aldrich) was dissolved in DI water (200 mL) and stirred overnight at 85 °C until the PVA was completely dissolved. The PVA solution was stored at room temperature for further use.

Preparation of Cross-Linked PVA/CNF Aerogels. The CNF solution (175 g, 0.74 wt %), PVA solution (19.5 mL, 0.1 g mL^{-1}), and DI water (15.5 mL) were mixed together in a flask under vigorous stirring for 1 h. The weight ratio between the PVA and CNF was 3:2. Then, a glutaraldehyde solution (1.3 mL, 25 wt %, Sigma-Aldrich) and sulfuric acid (1.3 mL, 1.0 vol %, Sigma-Aldrich) were added to the PVA/CNF solution[56] whose pH ranged from 4 to 6. The resulting PVA/CNF solution was subjected to mechanical stirring for 1 h, then sonicated in an ultrasonic bath for another hour, and finally placed in a vacuum oven to remove any residual air bubbles. The obtained aqueous gel was transferred into 50 mL centrifuge tubes and subsequently cross-linked/cured in an oven at 75 °C for 3 h. The cross-linked/cured aqueous gel was stored in a 4 °C refrigerator overnight to avoid macroscopic fracture during the freezing step.

Preparation of PVA/CNF Aerogels with an Aligned Microtubular Porous Structure. A 500 mL beaker was placed into an expandable polystyrene (EPS) box that was filled with dry ice to keep the temperature constant. The centrifuge tube containing the PVA/CNF aqueous gel was suspended on the rim of the beaker. The PVA/CNF aqueous gel was unidirectionally frozen by adding the dry ice−acetone solution (−78 °C) into the beaker at a constant rate (30 cm h^{-1}). The resulting frozen sample was freeze-dried in a lyophilizer at a condenser temperature of −87.0 °C under vacuum (0.0014 mbar) for 4 days to produce the aerogels with a unidirectionally aligned microtubular porous structure. The final cylindrical aerogel products with a diameter of 25 mm were stored in a desiccator for further characterization.

Preparation of Superhydrophobic PVA/CNF Aerogels. The superhydrophilic surface of the PVA/CNF aerogels was converted to a superhydrophobic surface via silanization using a thermal chemical vapor deposition (CVD) technique.[55] A glass vial containing methyltrichlorosilane (1 mL, 99 wt %, Sigma-Aldrich) was placed in a vacuum desiccator together with the aerogel samples. The desiccator was well sealed and then vacuumed to 80 kPa below atmospheric pressure. The desiccator was then heated inside a 50 °C oven for 48 h. After the desiccator was taken out of the oven, nitrogen gas was delivered into the desiccator overnight to exchange all of the undesired gas in it, including unreacted silane and the byproduct HCl.

Preparation of PDMS/Aerogel Composites. The PDMS prepolymer (20 g) (184 Silicone Elastomer Part A, Dow Corning) and curing agent (2 g) (Part B, Dow Corning) were mixed in a 50 mL centrifuge tube with a weight ratio of 10:1 according to the manufacturer's instructions. Afterward, the centrifuge tube was placed in a vacuum desiccator to degas for 10−15 min. Then, the PVA/CNF aerogel was backfilled with PDMS using a vacuum-assisted liquid filling method. Specifically, the silanized superhydrophobic PVA/CNF aerogel was put into the centrifuge tube containing the degassed PDMS prepolymer/curing agent mixture and was allowed to float on top of it. This centrifuge tube, which contained both the PDMS mixture and the aerogel, was then transferred into a laboratory-made vacuum chamber placed in an ice bath to prevent the PDMS from cross-linking during the filling stage. After up to 4 days of filling, the resulting PDMS/aerogel composite precursor was then cured at 125 °C for 30 min.

Characterization Methods. For all of the tests described below, at least three tests were measured for each sample, and the average results were reported. The densities of the aerogels were calculated according to the measurements of their masses and volume. The microstructure of the aerogels was investigated using a scanning electron microscope (SEM, LEO GEMINI 1530). The surface of the SEM specimen was sputtered with a thin gold layer. The FTIR spectra were obtained on a Tensor 27 spectrometer (Bruker Daltonics Inc., USA) with 4 cm^{-1} resolution at room temperature. The water contact angle was measured using a contact angle goniometer (OCA 15/20, Future Digital Scientific Corp., USA) at room temperature. The volume of the water droplet was 4.0 μL, and the contact angle was determined 10 s after the water droplet was deposited on the specimen's surface. The reported values of the contact angles were measured at five different positions on each specimen. Compression and tensile testing were conducted using an Instron (model 5967) at room temperature. The compression strain rate was set at 10% min^{-1} for the tests. The specimens were cut into cubes (10 × 10 × 10 mm^3) for compression testing. The tension rate was set at 5 mm min^{-1}. The specimens for the tensile tests were cut into cuboids (20 × 10 × 1 mm^3). Thermal stability measurements were carried out using a thermogravimetric analyzer (TGA, Q 50 TA Instruments, USA) from 30 to 900 °C at a 10 °C min^{-1} heating rate under N_2 protection. The samples were pretreated at 100 °C for 1 h to remove moisture before the TGA test.

Calculation of Aerogel Porosity, PDMS Filling Ratio, and Aerogel Content in the PDMS/Aerogel Composites. The density of the solid materials (ρ_s) was calculated based on the solid density of each component and their weight ratios and used in the formulation according to eq 1

$$\rho_s = \frac{1}{(W_{silane}/\rho_{silane}) + (W_{CNF}/\rho_{CNF}) + (W_{PVA}/\rho_{PVA})} \quad (1)$$

where W was the weight percentage of the different components, and ρ_{CNF}, ρ_{PVA}, and ρ_{silane} were the solid densities of CNF, PVA, and silane,

DOI: 10.1021/acsami.5b01679
ACS Appl. Mater. Interfaces 2015, 7, 7436−7444

respectively. The densities of the CNF, PVA, and silane used for this study were 1460, 1269, and 1273 kg m^{-3}, respectively, according to the manufacturer's data sheet.

The porosity (P) of aerogels was calculated according to eq 2

$$P(\%) = (1 - \rho/\rho_s) \times 100\% \quad (2)$$

where ρ was the density of the aerogel, and ρ_s was the density of the solid material.

The filling ratio (F) of PDMS into the PVA/CNF aerogel was calculated according to eq 3

$$F(\%) = (\rho_C - \rho_A)/\rho_P \times 100\% \quad (3)$$

where ρ_C, ρ_A, and ρ_P were the densities of the PDMS/aerogel composite, aerogel phase in the PDMS/aerogel composite, and pure PDMS, respectively.

The weight percentage of aerogel in the PDMS/aerogel composite was calculated according to eq 4

$$W_A(\%) = \rho_A/\rho_C \times 100\% \quad (4)$$

where ρ_A and ρ_C were the densities of the aerogel phase in the PDMS/aerogel composite and the PDMS/aerogel composite, respectively.

RESULTS AND DISCUSSION

Microstructure of PVA/CNF Aerogels with an Aligned Microtubular Porous Structure. PVA/CNF aerogels with unidirectional porous structures were successfully fabricated using a unidirectional freeze-drying process at a dry ice/acetone rising rate of 30 cm h^{-1}. Figures 1(a) and (b) show the microstructures of the PVA/CNF aerogels before surface modification. Figure 1(a) shows the microstructure of the aerogel cross section perpendicular to the vertical cooling direction having a polygonal porous structure with an average pore size around 37.8 ± 16.5 μm. Figure 1(b) shows the microstructure of the aerogel cross section parallel to the vertical cooling direction with clear tubular porous microchannels. This unidirectional porous structure was attributed to the preferential growth of the ice crystals along the cooling/freezing direction. The subsequent sublimation of the vertically orientated ice crystals led to the formation of the vertically aligned microtubular porous structure.

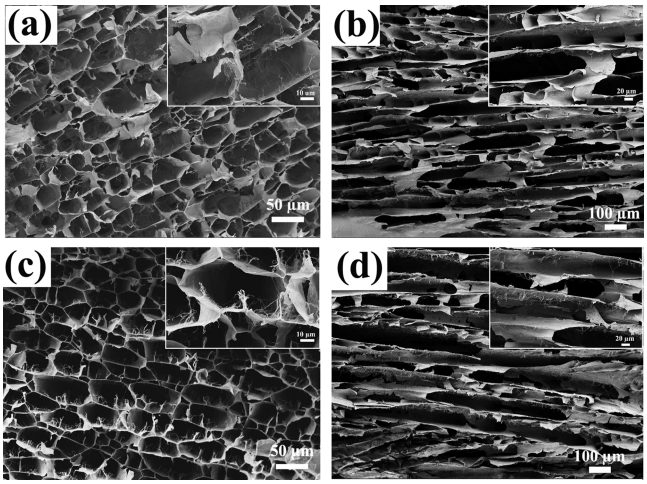

Figure 1. Typical SEM images of PVA/CNF aerogels: (a) uncoated and (c) silane-coated PVA/CNF aerogel cross section perpendicular to the freezing direction; (b) uncoated and (d) silane-coated aerogel cross section parallel to the freezing direction.

In order to obtain hydrophobic aerogels, methyltrichlorosilane in a gaseous phase was used to reach the hydroxyl groups present on the porous surface of the aerogel through a simple thermal chemical vapor deposition method. Figures 1(c) and (d) show the microstructures of the PVA/CNF aerogels after silane coating. The silane coating step did not affect the pore structure of the aerogels in terms of the pore size and shape. However, more nanofiber-like structures appeared on the surface of the cellular wall, as shown in Figure 1(c) and the enlarged images inserted in Figures 1(c) and (d). During the silanization process, two types of coating structures may have been formed.[57] The formation of these two types of structures is schematically shown in Figure 2. The hydroxyl groups shown in Figure 2 can be from either PVA or CNFs. One was a cross-linked polymeric fiber structure which was formed by vertical polymerization of organosilanes under humid conditions (i.e., with a relative humidity of 35% to 65%). The other was a covalently attached monolayer coating structure formed by the horizontal polymerization of self-assembled monolayer silane molecules under dry reaction conditions. Thus, the nanofiber-like structures that appeared on the silane-treated aerogel surfaces were likely due to the formation of silicone nanofilaments by the vertical polymerization of a small portion of silane.[55,57−59] Although the silanization reaction was conducted under a dry condition, since both PVA and CNF are highly hydrophilic, it was likely that a small amount of moisture was present in the aerogel, triggering the vertical polymerization. However, it is believed that the horizontal polymerization was dominant in this case due to the dry reaction condition. Horizontal polymerization results in the formation of a covalently attached silane monolayer coating which not only affords a completely hydrophobic aerogel surface but also builds a strong cross-linked Si−O−Si monolayer coating which would enhance the mechanical properties of the porous matrix.[60] Furthermore, the molecular structure of this silane-coating layer is similar to that of PDMS, which would greatly reduce the incompatibility between the PDMS and PVA/CNF aerogel interfaces.

The physical properties of the PVA/CNF aerogels before and after silane coating are summarized in Table 1. The densities of the PVA/CNF aerogels before and after the silane coating were 16.08 and 17.79 kg m^{-3}, respectively. Both of these aerogels exhibited a very high porosity (>98%). The density of the coated aerogel increased about 10%.

FTIR Spectra and Surface Wettability of PVA/CNF Aerogels. Successful silanization on the porous surface of the PVA/CNF aerogels was also confirmed by FTIR analysis (Figure 3). The FTIR spectrum showed two absorption bands located at ∼781 and ∼1271 cm^{-1}, which were ascribed to the characteristic vibrations of Si−O−Si and C−Si asymmetric stretching, respectively, in the C−Si−O units.[60] The typical absorption bands of the Si−O−Si bonds present in the siloxane compounds in the 1000−1130 cm^{-1} region overlapped with the C−O bonds of cellulose.[61]

The surface wettability of the PVA/CNF aerogel before and after silane coating was studied via a contact angle measurement. The pristine PVA/CNF aerogel was superhydrophilic due to the abundant hydroxyl groups present in both PVA and CNFs.

As shown in Figure 4(a), for the pristine PVA/CNF aerogel (i.e., before silane coating), the 4 μL water droplet was completely absorbed within only 0.3 s. In contrast, the silane-coated aerogels became superhydrophobic, on which the water

DOI: 10.1021/acsami.5b01679
ACS Appl. Mater. Interfaces 2015, 7, 7436−7444

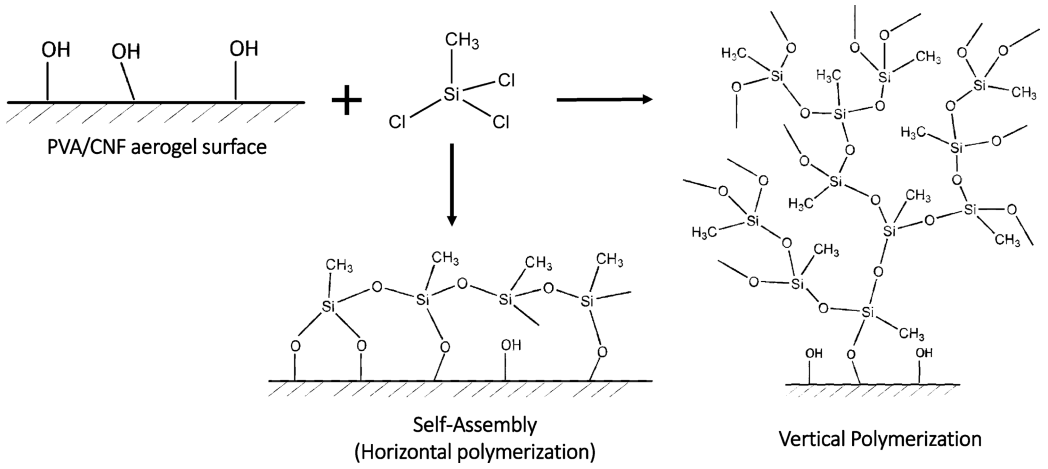

Figure 2. Possible reaction mechanisms between methyltrichlorosilane and the PVA/CNF aerogel surfaces.

Table 1. Physical Properties of Aerogels with and without Silane Coating

	density (kg m^{-3})	porosity (%)
uncoated aerogel	16.08 ± 1.14	98.8%
silane aerogel	17.79 ± 0.83	98.7%

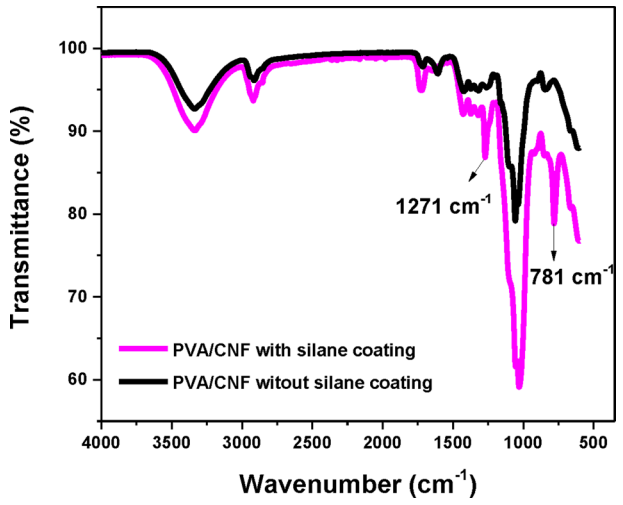

Figure 3. FTIR spectra of the PVA/CNF aerogels with and without a silane coating.

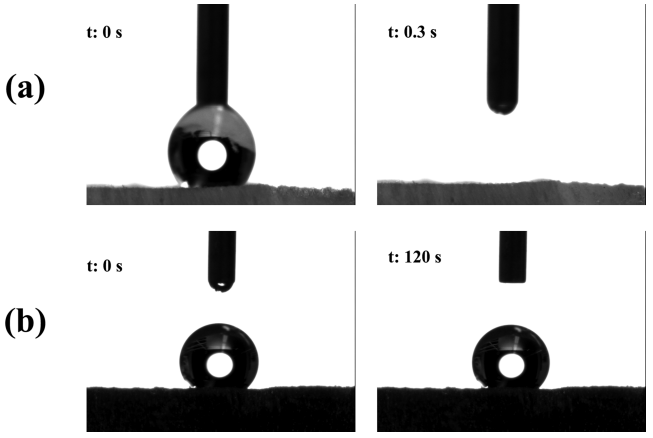

Figure 4. Water contact angle measurements of the PVA/CNF aerogels: (a) uncoated aerogel and (b) silane-coated aerogel.

droplet maintained its initial contact angle as well as its round shape after 120 s. The contact angle of the water droplet was 141.8° ± 1.4°.

As mentioned previously, in order to completely fill the PVA/CNF aerogels with PDMS, a unidirectional freeze-drying process was employed to create numerous tubular microchannels. The microtube-like porous structure was generated via the aligned ice crystal templates formed during unidirectional freezing. The ice was crystallized and grown along the freezing direction due to constitutional supercooling.[52,62] When the degree of supercooling was increased during the crystallization process, Mullins–Sekerka instability occurred and created crystals with cellular (microtube-like) or dendritic (ladder-like) structures.[52] The aligned microchannels present in the porous aerogels provided a natural passage to gradually draw PDMS molecules from one end of the porous structure to the other end. Therefore, these tubular microchannels not only reduced the "dead end" space in the whole aerogel structure but also helped to avoid the trapping of air bubbles caused by irregular porous structures. Additionally, the vacuum applied on this polymer filling system was able to rapidly vent out the gas molecules, thereby facilitating the PDMS to fully fill the high porosity aerogel.

Microstructure of PDMS-Filled Aerogel Composites. One major goal of this study is to establish a new method of producing bicontinuous CNF-based polymer nanocomposites. This method should be applicable for a wide range of thermoset resins. PDMS was chosen for this study since it is one of the most widely used thermoset resins. Figure 5 shows the microstructures of PVA/CNF aerogels before and after being filled with PDMS. As a control, a lower magnification PVA/CNF aerogel SEM image is shown in Figure 5(a). The viscosity of the uncured SYLGARD 184 was very high at 3500 mPa·s after mixing part A with part B according to the manufacturer's data sheet. As shown in Figure 5(b), all polygonal pores seemed to be fully filled by PDMS without the visible filling defects or air bubbles found in the PDMS/aerogel composite. The medium and higher magnification images of the PDMS/aerogel composite shown in Figures 5(c) and (d) suggest strong interfacial bonding between the PDMS phase and aerogel walls. The thin aerogel wall, which was approximately 210 nm in thickness, is shown in Figure 5(d), and no interfacial cracks were observed under such a high

DOI: 10.1021/acsami.5b01679
ACS Appl. Mater. Interfaces 2015, 7, 7436–7444

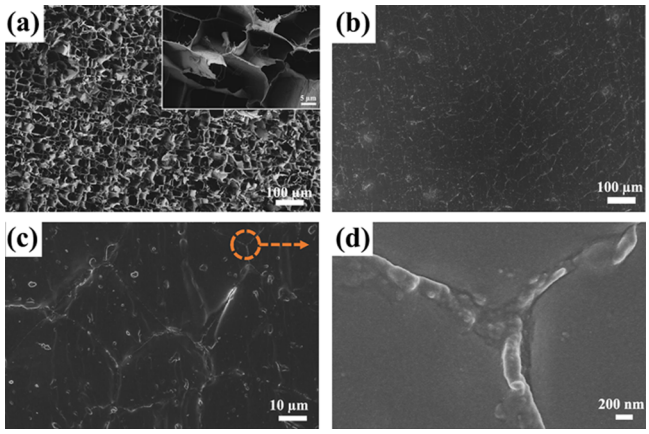

Figure 5. SEM images of the PVA/CNF aerogel before and after being filled with PDMS: (a) aerogel without PDMS, (b) a lower magnification, (c) a medium magnification, and (d) a high magnification image of the aerogel after being filled with PDMS.

magnification. This demonstrated that the PVA/CNF aerogel surfaces after methyltrichlorosilane treatment had excellent surface compatibility with PDMS molecules.

The microscope images of the PDMS/aerogel composites are presented in Figure 6. For optical microscope observation,

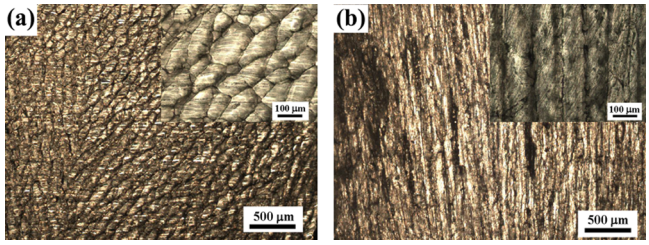

Figure 6. Optical microscopy images of the PDMS/aerogel composites: (a) cross section perpendicular to the freezing direction and (b) cross section parallel to the freezing direction.

the cured PDMS/aerogel composites were cut into slices with a thickness of about 0.2 mm in both directions (perpendicular and parallel to the freezing/cooling direction). Compared to the SEM images, the PVA/CNF aerogel networks were much clearer in the microscopic images. From Figure 6(a), the aerogel walls, or aerogel networks, as well as the transparent PDMS phase in the cross section perpendicular to the freezing direction can be easily observed. Figure 6(b) clearly shows the aligned microtubular structure of the PVA/CNF aerogel, and the inset image of Figure 6(b) shows the parallel aerogel walls. All of these SEM and optical images clearly show that complete PDMS filling in silane-treated aerogels has been achieved as a result of the unique microtubular porous structure of the aerogel and the excellent surface compatibility between PDMS and the surface-modified aerogel.

Table 2 shows the densities and filling ratio of the PDMS/aerogel composites and pure PDMS. The resulting filling ratio

Table 2. Physical Properties of Pure PDMS and PDMS/Aerogel Composites

	density (kg m^{-3})	filling ratio (%)
pure PDMS	1006.7 ± 6.3	−−
PDMS/aerogel composite	1022.1 ± 53.3	99.8%

based on eq 3 was 99.8%. On the basis of the porosity of the silane-coated aerogel and the filling ratio of PDMS, as shown in Table 1 and Table 2, the volume percentage of PDMS in the composites was around 98 vol %. The weight percentage of the aerogel in the PDMS/aerogel composite was calculated to be 1.7 wt % according to eq 4. Due to the difficulties of measuring the actual density of the aerogel within the PDMS/aerogel composite, the value of ρ_A used in these equations was the density of the silane-coated PVA/CNF aerogel, which is listed in Table 1. This substitution may cause a slightly lower value in the calculated filling ratio (as compared to the actual filling ratio, which should be 100% according to the SEM analyses) and a slightly higher value for the weight percentage of aerogel in the PDMS/aerogel composite since the volume of the aerogel after being filled with PDMS would be slightly higher.

Compressive and Tensile Properties of Aerogel/PDMS Composites. The compressive stress−strain curves of silane-coated aerogels, pure PDMS, and the PDMS/aerogel composites are shown in Figure 7. Since the aerogel had an anisotropic structure, its compressive stress and Young's modulus in the aligned direction (i.e., along the freezing/cooling direction) was much higher than those in the perpendicular direction (i.e., perpendicular to the cooling direction) as shown in Figure 7(b). The "*a-*" and "*p-*" in front of the sample name stand for the "aligned direction" and "perpendicular direction," respectively, as shown in Figure 7(c). Figure 7(a) clearly shows that the compressive properties of the aerogel/PDMS composites improved significantly in comparison with both pure PDMS and the original unfilled aerogels. The compressive stresses and Young's moduli of the aerogels, pure PDMS, and PDMS/aerogel composites are listed in Table 3. In both directions (i.e., both the aligned and perpendicular direction), the Young's moduli, as well as the compressive stresses at 10% and 30% strain of the PDMS/aerogel composite, were all more than 2-fold higher than those of pure PDMS. This improvement in mechanical properties demonstrated that, on one hand, the silane coating layer, which is similar to the molecular structure of PDMS, evidently increased the interfacial compatibility between the PDMS and PVA/CNF aerogel interface, while on the other hand, the aerogel played an important role as a rigid continuous filler network, which could result in efficient mechanical reinforcement.[46−48] According to the porosity of aerogel (i.e., 98.7%) and assuming complete filling, the volume fraction of aerogel should be about 1.3 vol %. Therefore, the reinforcing effect of the aerogel is quite efficient compared with commonly used reinforcing fillers, such as nanoclay,[63] carbon nanotubes,[2] and carbon black.[64]

Interestingly, the differences in the compressive properties of the unfilled aerogels along the aligned and perpendicular directions were much greater than those of the PDMS/aerogel composites. For instance, the Young's modulus and compressive stress at 10% and 30% strain of the unfilled aerogel in the aligned direction was more than 26-, 17-, and 10-fold higher than those in the perpendicular direction. However, the Young's modulus and compressive stress of the PDMS/aerogel composite in the aligned direction were just slightly higher than those in the perpendicular direction as shown in Table 3.

The efficient mechanical reinforcement effect was also validated through tensile testing. The tensile stress−strain curves of the PDMS/aerogel composites and pure PDMS are shown in Figure 8, and the Young's modulus and tensile stress at a specific strain are listed in Table 4. The Young's modulus of

DOI: 10.1021/acsami.5b01679
ACS Appl. Mater. Interfaces 2015, 7, 7436−7444

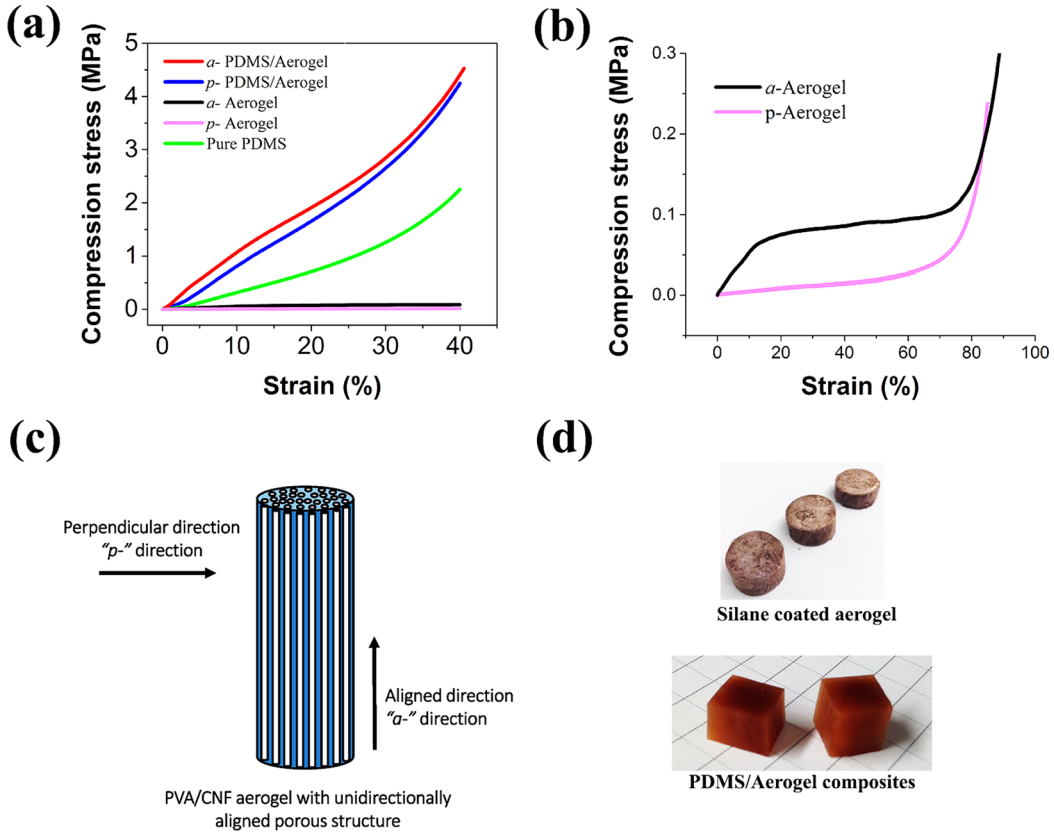

Figure 7. Compressive stress–strain curves of the PVA/CNF aerogels: (a) before and after being filled with PDMS, (b) enlarged stress–strain curves of the PVA/CNF aerogels before being filled with PDMS, (c) schematic picture of the PVA/CNF aerogel in which "*p*-" and "*a*-" directions are marked, and (d) pictures of the silane-coated aerogel and PDMS/aerogel composites.

Table 3. Compressive Strength and Young's Modulus of Pure PDMS, Unfilled Aerogels, and PDMS/Aerogel Composites

	Young's modulus (MPa)	compression stress at 10% strain (MPa)	compression stress at 30% strain (MPa)
pure PDMS	3.81 ± 0.02	0.39 ± 0.10	1.38 ± 0.13
a-PDMS/aerogels[a]	10.44 ± 0.18	1.06 ± 0.01	2.83 ± 0.06
p-PDMS/aerogels[a]	9.60 ± 0.73	0.82 ± 0.03	2.73 ± 0.09
a-aerogels[a]	0.79 ± 0.31	0.08 ± 0.03	0.10 ± 0.01
p-aerogels[a]	0.03 ± 0.01	$4.5 \times 10^{-3} \pm 0.5 \times 10^{-3}$	0.010 ± 0.001

[a]"*a*-" and "*p*-" stand for "aligned direction" and "perpendicular direction," respectively.

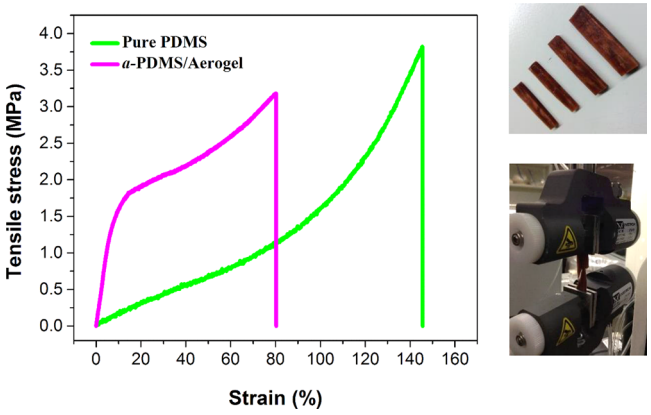

Figure 8. Tensile stress–strain curves of the PVA/CNF aerogels before and after being filled with PDMS.

the PDMS/aerogel composite was more than 15-fold higher than that of pure PDMS. The tensile stress of the PDMS/aerogel composite at 20% and 40% strain was more than 6- and 4-fold higher than those of the pure PDMS, respectively. However, the elongation-at-break for the PDMS/aerogel composite (80.4%) was lower than that of the pure PDMS (i.e., 150.9%). This was due to the fact that at room temperature both PVA and CNFs are more brittle than PDMS. Regardless, the PDMS/aerogel composite exhibited an excellent set of mechanical properties, namely, much higher compressive and tensile strengths and moduli as well as a reasonable elongation-at-break (80.4%).

Thermal Stability of PVA/CNF Aerogels and PDMS/Aerogel Composites. The thermal stabilities of the PVA/CNF aerogels before and after silane treatment, pure PDMS, and PDMS/aerogel composites were measured by TGA in nitrogen from 30 to 900 °C, as shown in Figure 9. The thermal stability of the aerogel was slightly improved after silane treatment. The maximum decomposition temperature of PVA and CNF after silane coating was increased from 262 to 291 °C and from 463 to 495 °C, respectively. This might have been because the thin silane layer retarded the thermal decomposition of the aerogels.[65]

DOI: 10.1021/acsami.5b01679
ACS Appl. Mater. Interfaces 2015, 7, 7436–7444

Table 4. Tensile Strength and Young's Modulus of Pure PDMS and PDMS/Aerogel Composites

	Young's modulus (MPa)	tensile stress at 20% strain (MPa)	tensile stress at 40% strain (MPa)	elongation-at-break (%)
pure PDMS	1.45 ± 0.05	0.30 ± 0.02	0.52 ± 0.03	150.9 ± 7.2
a-PDMS/aerogels	22.2 ± 0.8	1.91 ± 0.02	2.18 ± 0.05	80.4 ± 2.6

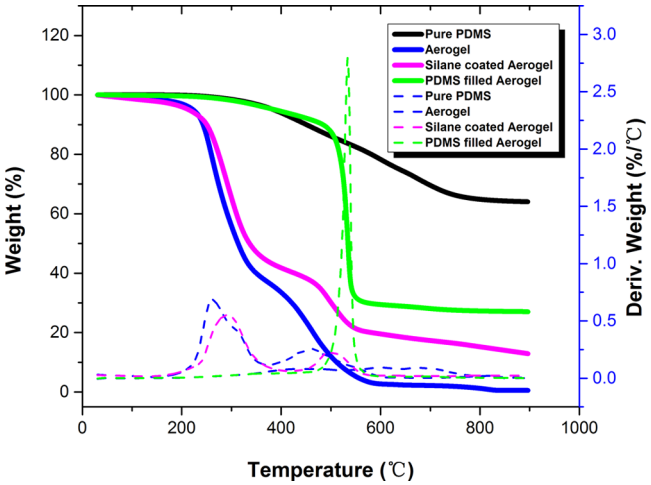

Figure 9. Thermogravimetric (TG) and derivative thermogravimetric (DTC) curves of the PVA/CNF aerogels before and after being filled with PDMS.

As shown in Figure 9, the PDMS/aerogel composite experienced a dramatic decomposition at 534 °C. In contrast, the decomposition of pure PDMS was much less apparent. This may be attributed to the much higher specific surface area of the PDMS phase after the decomposition of the aerogel network as compared to pure PDMS, making it much more susceptible to thermal degradation. A similar dramatic decomposition of PDMS was also reported in the PDMS/PVA composite.[66]

CONCLUSIONS

Superhydrophobic PVA/CNF aerogels were prepared by a unidirectional freeze-drying process followed by thermal chemical vapor deposition of methyltrichlorosilane. The PVA/CNF aerogel had an anisotropic structure. The aerogel exhibited a polygonal porous structure perpendicular to the freezing direction but had an aligned microtubular porous structure along the freezing direction. Completely filled PDMS/aerogel composites were obtained through a vacuum-assisted process. Owing to the excellent compatibility between the PDMS, the silane-coated PVA/CNF aerogel interface, and the rigid continuous aerogel reinforcing network, the mechanical properties of the PDMS/aerogel improved significantly. The compressive Young's modulus and the compressive stress at specific strains of the PDMS/aerogel composites were more than 2-fold higher than those of pure PDMS. The tensile modulus of the PDMS/aerogel composite increased more than 15-fold compared with pure PDMS. Thus, this study may offer a novel method to fabricate reinforcing polymer composites or prepare polymer composites with bicontinuous structures.

AUTHOR INFORMATION

Corresponding Authors

*E-mail: sgong@engr.wisc.edu (S. G.).
*E-mail: xiahs@scu.edu.cn (H. X.).

Notes

The authors declare no competing financial interest.

ACKNOWLEDGMENTS

The authors would like to acknowledge the financial support from the University of Wisconsin−Madison, the Wisconsin Institute for Discovery (WID), and the China Scholarship Council (CSC).

REFERENCES

(1) Ovid'ko, I. A. Enhanced Mechanical Properties of Polymer-Matrix Nanocomposites Reinforced by Graphene Inclusions: A Review. *Rev. Adv. Mater. Sci.* **2013**, *34* (1), 19−25.
(2) Coleman, J. N.; Khan, U.; Blau, W. J.; Gun'ko, Y. K. Small but Strong: A Review of the Mechanical Properties of Carbon Nanotube-Polymer Composites. *Carbon* **2006**, *44* (9), 1624−1652.
(3) Bauhofer, W.; Kovacs, J. Z. A Review and Analysis of Electrical Percolation in Carbon Nanotube Polymer Composites. *Compos. Sci. Technol.* **2009**, *69* (10), 1486−1498.
(4) Porter, D.; Metcalfe, E.; Thomas, M. J. K. Nanocomposite fire retardants - A review. *Fire Mater.* **2000**, *24* (1), 45−52.
(5) Liu, J.; Boo, W. J.; Clearfield, A.; Sue, H. J. Intercalation and Exfoliation: A Review on Morphology of Polymer Nanocomposites Reinforced by Inorganic Layer Structures. *Mater. Manuf. Process.* **2006**, *21* (2), 143−151.
(6) Miao, C. W.; Hamad, W. Y. Cellulose Reinforced Polymer Composites and Nanocomposites: A Critical Review. *Cellulose* **2013**, *20* (5), 2221−2262.
(7) Liu, Y. D.; Kumar, S. Polymer/Carbon Nanotube Nano Composite Fibers-A Review. *ACS Appl. Mater. Interfaces* **2014**, *6* (9), 6069−6087.
(8) Stefanescu, E. A.; Daranga, C.; Stefanescu, C. Insight into the Broad Field of Polymer Nanocomposites: From Carbon Nanotubes to Clay Nanoplatelets, via Metal Nanoparticles. *Materials* **2009**, *2* (4), 2095−2153.
(9) Jin, C. Z.; Wang, Y. J.; Wei, H. S.; Tang, H. L.; Liu, X.; Lua, T.; Wang, J. H. Magnetic Iron Oxide Nanoparticles Coated by Hierarchically Structured Silica: A Highly Stable Nanocomposite System and Ideal Catalyst Support. *J. Mater. Chem. A* **2014**, *2* (29), 11202−11208.
(10) Wang, L. J.; He, X. J.; Wilkie, C. A. The Utility of Nanocomposites in Fire Retardancy. *Materials* **2010**, *3* (9), 4580−4606.
(11) Morgan, A. B. Flame Retarded Polymer Layered Silicate Nanocomposites: A Review of Commercial and Open Literature Systems. *Polym. Adv. Technol.* **2006**, *17* (4), 206−217.
(12) Song, F. F.; Li, X. Q.; Wang, Q.; Liao, L. Q.; Zhang, C. Nanocomposite Hydrogels and Their Applications in Drug Delivery and Tissue Engineering. *J. Biomed. Nanotechnol.* **2015**, *11* (1), 40−52.
(13) Liu, D. F.; Makila, E.; Zhang, H. B.; Herranz, B.; Kaasalainen, M.; Kinnari, P.; Salonen, J.; Hirvonen, J.; Santos, H. A. Nanostructured Porous Silicon-Solid Lipid Nanocomposite: Towards Enhanced Cytocompatibility and Stability, Reduced Cellular Association, and Prolonged Drug Release. *Adv. Funct. Mater.* **2013**, *23* (15), 1893−1902.
(14) Hoare, T.; Timko, B. P.; Santamaria, J.; Goya, G. F.; Irusta, S.; Lau, S.; Stefanescu, C. F.; Lin, D. B.; Langer, R.; Kohane, D. S. Magnetically Triggered Nanocomposite Membranes: A Versatile Platform for Triggered Drug Release. *Nano Lett.* **2011**, *11* (3), 1395−1400.

DOI: 10.1021/acsami.5b01679
ACS Appl. Mater. Interfaces 2015, 7, 7436−7444

(15) Tan, C. W.; Tan, K. H.; Ong, Y. T.; Mohamed, A. R.; Zein, S. H. S.; Tan, S. H. Energy and Environmental Applications of Carbon Nanotubes. *Environ. Chem. Lett.* **2012**, *10* (3), 265−273.
(16) Oelhafen, P.; Schuler, A. Nanostructured Materials for Solar Energy Conversion. *Sol. Energy* **2005**, *79* (2), 110−121.
(17) Alturaif, H. A.; Alothman, Z. A.; Shapter, J. G.; Wabaidur, S. M. Use of Carbon Nanotubes (CNTs) with Polymers in Solar Cells. *Molecules* **2014**, *19* (11), 17329−17344.
(18) Klemm, D.; Heublein, B.; Fink, H. P.; Bohn, A. Cellulose: Fascinating Biopolymer and Sustainable Raw Material. *Angew. Chem., Int. Ed.* **2005**, *44* (22), 3358−3393.
(19) Klemm, D.; Kramer, F.; Moritz, S.; Lindstrom, T.; Ankerfors, M.; Gray, D.; Dorris, A. Nanocelluloses: A New Family of Nature-Based Materials. *Angew. Chem., Int. Ed.* **2011**, *50* (24), 5438−5466.
(20) Moon, R. J.; Martini, A.; Nairn, J.; Simonsen, J.; Youngblood, J. Cellulose Nanomaterials Review: Structure, Properties and Nanocomposites. *Chem. Soc. Rev.* **2011**, *40* (7), 3941−3994.
(21) Iwamoto, S.; Kai, W. H.; Isogai, A.; Iwata, T. Elastic Modulus of Single Cellulose Microfibrils from Tunicate Measured by Atomic Force Microscopy. *Biomacromolecules* **2009**, *10* (9), 2571−2576.
(22) Eichhorn, S. J.; Dufresne, A.; Aranguren, M.; Marcovich, N. E.; Capadona, J. R.; Rowan, S. J.; Weder, C.; Thielemans, W.; Roman, M.; Renneckar, S.; Gindl, W.; Veigel, S.; Keckes, J.; Yano, H.; Abe, K.; Nogi, M.; Nakagaito, A. N.; Mangalam, A.; Simonsen, J.; Benight, A. S.; Bismarck, A.; Berglund, L. A.; Peijs, T. Review: Current International Research into Cellulose Nanofibres and Nanocomposites. *J. Mater. Sci.* **2010**, *45* (1), 1−33.
(23) Javadi, A.; Srithep, Y.; Pilla, S.; Lee, J.; Gong, S.; Turng, L. S. Processing and Characterization of Solid and Microcellular PHBV/Coir Fiber composites. *Mater. Sci. Eng. C-Mater.* **2010**, *30* (5), 749−757.
(24) Pilla, S.; Gong, S. Q.; O'Neill, E.; Yang, L. Q.; Rowell, R. M. Polylactide-Recycled Wood Fiber Composites. *J. Appl. Polym. Sci.* **2009**, *111* (1), 37−47.
(25) Bledzki, A. K.; Gassan, J. Composites Reinforced with Cellulose Based Fibres. *Prog. Polym. Sci.* **1999**, *24* (2), 221−274.
(26) Saheb, D. N.; Jog, J. P. Natural Fiber Polymer Composites: A review. *Adv. Polym. Technol.* **1999**, *18* (4), 351−363.
(27) Khalil, H. P. S. A.; Bhat, A. H.; Yusra, A. F. I. Green Composites from Sustainable Cellulose Nanofibrils: A Review. *Carbohydr. Polym.* **2012**, *87* (2), 963−979.
(28) Siro, I.; Plackett, D. Microfibrillated Cellulose and New Nanocomposite Materials: a review. *Cellulose* **2010**, *17* (3), 459−494.
(29) Dufresne, A. Processing of Polymer Nanocomposites Reinforced with Polysaccharide Nanocrystals. *Molecules* **2010**, *15* (6), 4111−4128.
(30) Nakagaito, A. N.; Yano, H. The Effect of Fiber Content on the Mechanical and Thermal Expansion Properties of Biocomposites Based on Microfibrillated Cellulose. *Cellulose* **2008**, *15* (4), 555−559.
(31) Nakagaito, A. N.; Yano, H. The Effect of Morphological Changes from Pulp Fiber Towards Nano-scale Fibrillated Cellulose on the Mechanical Properties of High-Strength Plant Fiber Based Composites. *Appl. Phys. A-Mater.* **2004**, *78* (4), 547−552.
(32) Henriksson, M.; Berglund, L. A. Structure and properties of cellulose nanocomposite films containing melamine formaldehyde. *J. Appl. Polym. Sci.* **2007**, *106* (4), 2817−2824.
(33) Samir, M. A. S. A.; Alloin, F.; Sanchez, J. Y.; El Kissi, N.; Dufresne, A. Preparation of Cellulose Whiskers Reinforced Nanocomposites from an Organic Medium Suspension. *Macromolecules* **2004**, *37* (4), 1386−1393.
(34) Wu, Q. J.; Henriksson, M.; Liu, X.; Berglund, L. A. A High Strength Nanocomposite Based on Microcrystalline Cellulose and Polyurethane. *Biomacromolecules* **2007**, *8* (12), 3687−3692.
(35) Favier, V.; Chanzy, H.; Cavaille, J. Y. Polymer Nanocomposites Reinforced by Cellulose Whiskers. *Macromolecules* **1995**, *28* (18), 6365−6367.
(36) Malainine, M. E.; Mahrouz, M.; Dufresne, A. Thermoplastic Nanocomposites Based on Cellulose Microfibrils from Opuntia Ficus-indica Parenchyma Cell. *Compos. Sci. Technol.* **2005**, *65* (10), 1520−1526.
(37) Wang, B.; Sain, M. Dispersion of Soybean Stock-based Nanofiber in a Plastic Matrix. *Polym. Int.* **2007**, *56* (4), 538−546.
(38) Millon, L. E.; Wan, W. K. The Polyvinyl Alcohol-bacterial Cellulose System as a New Nanocomposite for Biomedical Applications. *J. Biomed. Mater. Res. B* **2006**, *79B* (2), 245−253.
(39) Samir, M. A. S. A.; Alloin, F.; Sanchez, J. Y.; Dufresne, A. Cellulose Nanocrystals Reinforced Poly(oxyethylene). *Polymer* **2004**, *45* (12), 4149−4157.
(40) Frone, A. N.; Berlioz, S.; Chailan, J. F.; Panaitescu, D. M. Morphology and Thermal Properties of PLA-cellulose Nanofibers Composites. *Carbohydr. Polym.* **2013**, *91* (1), 377−384.
(41) Kowalczyk, M.; Piorkowska, E.; Kulpinski, P.; Pracella, M. Mechanical and Thermal Properties of PLA Composites with Cellulose Nanofibers and Standard Size Fibers. *Composites, Part A* **2011**, *42* (10), 1509−1514.
(42) Ma, X. F.; Chang, P. R.; Yu, J. G. Properties of Biodegradable Thermoplastic Pea Starch/Carboxymethyl Cellulose and Pea Starch/Microcrystalline Cellulose Composites. *Carbohydr. Polym.* **2008**, *72* (3), 369−375.
(43) Sarazin, P.; Li, G.; Orts, W. J.; Favis, B. D. Binary and Ternary Blends of Polylactide, Polycaprolactone and Thermoplastic Starch. *Polymer* **2008**, *49* (2), 599−609.
(44) Belgacem, M. N.; Gandini, A. The Surface Modification of Cellulose Fibres for Use as Reinforcing Elements in Composite Materials. *Compos. Interfaces* **2005**, *12* (1−2), 41−75.
(45) Le Strat, D.; Dalmas, F.; Randriamahefa, S.; Jestin, J.; Wintgens, V. Mechanical Reinforcement in Model Elastomer Nanocomposites with Tuned Microstructure and Interactions. *Polymer* **2013**, *54* (5), 1466−1479.
(46) Chabert, E.; Bornert, M.; Bourgeat-Lami, E.; Cavaille, J. Y.; Dendievel, R.; Gauthier, C.; Putaux, U.; Zaoui, A. Filler-filler Interactions and Viscoelastic Behavior of Polymer Nanocomposites. *Mater. Sci. Eng., A* **2004**, *381* (1−2), 320−330.
(47) Dalmas, F.; Cavaille, J. Y.; Gauthier, C.; Chazeau, L.; Dendievel, R. Viscoelastic Behavior and Electrical Properties of Flexible Nanofiber Filled Polymer Nanocomposites. Influence of Processing Conditions. *Compos. Sci. Technol.* **2007**, *67* (5), 829−839.
(48) Tatou, M.; Genix, A. C.; Imaz, A.; Forcada, J.; Banc, A.; Schweins, R.; Grillo, I.; Oberdisse, J. Reinforcement and Polymer Mobility in Silica-Latex Nanocomposites with Controlled Aggregation. *Macromolecules* **2011**, *44* (22), 9029−9039.
(49) Wu, D. C.; Xu, F.; Sun, B.; Fu, R. W.; He, H. K.; Matyjaszewski, K. Design and Preparation of Porous Polymers. *Chem. Rev.* **2012**, *112* (7), 3959−4015.
(50) Tan, C. B.; Fung, B. M.; Newman, J. K.; Vu, C. Organic Aerogels with Very High Impact Strength. *Adv. Mater.* **2001**, *13* (9), 644−646.
(51) Pierre, A. C.; Pajonk, G. M. Chemistry of Aerogels and Their Applications. *Chem. Rev.* **2002**, *102* (11), 4243−4265.
(52) Kim, J. W.; Taki, K.; Nagamine, S.; Ohshima, M. Preparation of Poly(L-lactic acid) Honeycomb Monolith Structure by Unidirectional Freezing and Freeze-drying. *Chem. Eng. Sci.* **2008**, *63* (15), 3858−3863.
(53) Mukai, S. R.; Nishihara, H.; Shichi, S.; Tamon, H. Preparation of Porous TiO2 Cryogel Fibers Through Unidirectional Freezing of Hydrogel Followed by Freeze-drying. *Chem. Mater.* **2004**, *16* (24), 4987−4991.
(54) Wu, X.; Liu, Y.; Li, X.; Wen, P.; Zhang, Y.; Long, Y.; Wang, X.; Guo, Y.; Xing, F.; Gao, J. Preparation of Aligned Porous Gelatin Scaffolds by Unidirectional Freeze-drying Method. *Acta. Biomater.* **2010**, *6* (3), 1167−77.
(55) Zheng, Q. F.; Cai, Z. Y.; Gong, S. Q. Green Synthesis of Polyvinyl Alcohol (PVA)-Cellulose Nanofibril (CNF) Hybrid Aerogels and Their Use as Superabsorbents. *J. Mater. Chem. A* **2014**, *2* (9), 3110−3118.
(56) Zheng, Q. F.; Javadi, A.; Sabo, R.; Cai, Z. Y.; Gong, S. Q. Polyvinyl Alcohol (PVA)-Cellulose Nanofibril (CNF)-Multiwalled

DOI: 10.1021/acsami.5b01679
ACS Appl. Mater. Interfaces 2015, 7, 7436−7444

Carbon Nanotube (MWCNT) Hybrid Organic Aerogels with Superior Mechanical Properties. *Rsc. Adv.* **2013**, *3* (43), 20816−20823.
(57) Fadeev, A. Y.; McCarthy, T. J. Self-assembly is Not the Only Reaction Possible Between Alkyltrichlorosilanes and Surfaces: Monomolecular and Oligomeric Covalently Attached Layers of Dichloro- and Trichloroalkylsilanes on Silicon. *Langmuir* **2000**, *16* (18), 7268−7274.
(58) Zhang, J. P.; Seeger, S. Polyester Materials with Superwetting Silicone Nanofilaments for Oil/Water Separation and Selective Oil Absorption. *Adv. Funct. Mater.* **2011**, *21* (24), 4699−4704.
(59) Artus, G. R. J.; Jung, S.; Zimmermann, J.; Gautschi, H. P.; Marquardt, K.; Seeger, S. Silicone Nanofilaments and Their Application as Superhydrophobic Coating. *Adv. Mater.* **2006**, *18* (20), 2758−2762.
(60) Zhu, Q.; Chu, Y.; Wang, Z. K.; Chen, N.; Lin, L.; Liu, F. T.; Pan, Q. M. Robust Superhydrophobic Polyurethane Sponge as a Highly Reusable Oil-absorption Material. *J. Mater. Chem. A* **2013**, *1* (17), 5386−5393.
(61) Li, S. H.; Zhang, S. B.; Wang, X. H. Fabrication of Superhydrophobic Cellulose-based Materials Through a Solution-immersion Process. *Langmuir* **2008**, *24* (10), 5585−5590.
(62) Zhang, H. F.; Hussain, I.; Brust, M.; Butler, M. F.; Rannard, S. P.; Cooper, A. I. Aligned Two- and Three-dimensional Structures by Directional Freezing of Polymers and Nanoparticles. *Nat. Mater.* **2005**, *4* (10), 787−793.
(63) Hetzer, M.; De Kee, D. Wood/Polymer/Nanoclay Composites, Environmentally Friendly Sustainable Technology: A review. *Chem. Eng. Res. Des.* **2008**, *86* (10A), 1083−1093.
(64) Bokobza, L.; Rapoport, O. Silica and Carbon Black Reinforcement of Natural Rubber. *Macromol. Symp.* **2003**, *194*, 125−133.
(65) Javadi, A.; Zheng, Q. F.; Payen, F.; Javadi, A.; Altin, Y.; Cai, Z. Y.; Sabo, R.; Gong, S. Q. Polyvinyl Alcohol-Cellulose Nanofibrils-Graphene Oxide Hybrid Organic Aerogels. *ACS Appl. Mater. Interfaces* **2013**, *5* (13), 5969−5975.
(66) Lopes, A. L.; Augusto, F. Preparation and Characterization of Polydimethylsiloxane/Poly(vinylalcohol) Coated Solid Phase Microextraction Fibers Using Sol-gel Technology. *J. Chromatogr. A* **2004**, *1056* (1−2), 13−19.

DOI: 10.1021/acsami.5b01679
ACS Appl. Mater. Interfaces 2015, 7, 7436−7444